Available online at www.sciencedirect.com
SCIENCE DIRECT
Chemical Physics 325 (2006) 99–112
Chemical Physics
www.elsevier.com/locate/chemphys

The transport gap of organic semiconductors studied using the combination of direct and inverse photoemission

Dietrich R.T. Zahn *, Gianina N. Gavrila, Mihaela Gorgoi

Halbleiterphysik, Institut für Physik, Technische Universität Chemnitz, Physics, Reichenhainer Strasse 70, D-09107 Chemnitz, Germany

Received 24 October 2005; accepted 4 February 2006
Available online 2 March 2006

Abstract

The combination of valence band photoemission and inverse photoemission spectroscopy is applied to study the densities of occupied and unoccupied states of perylene derivative and phthalocyanine organic layers on inorganic semiconductors. The ionisation energies and electron affinities are determined and it is proposed that the transport gap of the materials can be evaluated from the distance of the HOMO and LUMO edges. The resulting values for the transport gap which are somewhat smaller than other published data are in good agreement with e.g. electrical measurements. The experimental spectra are compared with simulated ones obtained by density functional theory calculations.

Keywords: Organic semiconductors; Phthalocyanine; Perylene derivatives; Photoemission; Inverse photoemission; Transport gap

1. Introduction

Over the last few years organic semiconductors have attracted an increasing technological interest which is accompanied by a significant progress in fundamental research related to these materials. There are two types of organic materials used in semiconducting applications: polymers and low molecular weight materials [1]. While polymers tend to form disordered phases, small molecules often show ordered crystalline structures. In this work, we concentrate on molecular crystals consisting of small planar molecules.

The interest in the semiconducting properties of such organic molecules has intensified significantly in recent years and these materials have already appeared in a range of commercial applications. In spite of this rapid progress, the precise relationship between molecular and electronic structure and device performance is still not fully understood and there remains a need for detailed studies of model systems based on both polymers and small molecules [2,3]. Very thin layers of small organic molecules can be grown with high precision in ultra-high vacuum (UHV), which makes this class of materials ideal for studies of fundamental interface properties using, e.g. electron-based experimental techniques.

Earlier studies of molecular adsorption on low index faces of inorganic semiconductors suggested that a passivated surface is beneficial for ordered growth. It was found that, e.g. PTCDA forms ordered layers on GaAs(0 0 1) if the surface is passivated by a Se monolayer [4]. It was proposed that the GaAs surface bonds are saturated by Se and the organic molecules attach through weak van der Waals bonding. As a result of this weak interaction, the molecules arrange into an ordered, quasi-epitaxial overlayer. Efficient transport of charge through a semiconductor film requires the film to be continuous and ordered. Highly oriented films typically result in higher carrier mobilities than randomly oriented crystalline or amorphous films. One major advantage of organic molecules is that they can be tailored, i.e. their properties can be tuned by changing the molecular structure, e.g. via adding specific functional groups.

As noted by Dimitrakopoulos and Malenfant in their review [5] industrial emphasis is shifting away from organic

* Corresponding author. Tel.: +49 3715313036.
E-mail address: zahn@physik.tu-chemnitz.de (D.R.T. Zahn).

0301-0104/$ - see front matter © 2006 Elsevier B.V. All rights reserved.
doi:10.1016/j.chemphys.2006.02.003

semiconductor testing and more toward manufacturing process development. From the perspective of material science, there remain a number of unanswered questions concerning the performance of organic based devices. Over the past years, however, surface science has begun to play an important role in developing a more basic understanding of organic materials and their interfaces such as inorganic semiconductor/organic [6–8], metal/organic [9–12] or organic/organic interfaces [13–17]. Investigations of these interfaces are performed by means of various techniques such as optical and/or vibrational spectroscopies, but mainly by means of electron spectroscopies. The device performance is most affected by an efficient charge transfer across the interface. While charge transport through an organic layer critically depends on the choice of organic molecule, the structure and thickness of the organic film and on the preparation method, the most important factors that control the charge injection process are the energy barrier which the charge carrier has to overcome at the interfaces. Therefore, the starting point in the description of the interface is to define the relevant electronic levels and their alignment relative to the same reference (Fermi level). The most direct and successful methods for the determination of energy level positions and alignment are valence band photoemission spectroscopy (VB-PES) and inverse photoemission spectroscopy (IPES). VB-PES provides information on the density of occupied states while IPES provides information on the density of unoccupied states. Hence, a complete picture of the electronic properties, i.e. ionization energy (IE), work function (ϕ), energy position of the highest occupied molecular orbital (HOMO), electron affinity (EA) and energy position of the lowest unoccupied molecular orbital (LUMO) can only be achieved when UPS and IPES are employed in combination.

Among the many studies of molecular adsorption on a range of substrate surfaces, two main types of molecules have emerged as prototypes – perylene derivatives (e.g. 3,4,9,10-perylenetetracarboxylic dianhydride (PTCDA)) and phthalocyanines (e.g. copper phthalocyanine (CuPc)). In addition to their wide use in organic semiconductor devices, their properties have proven attractive in the field of conventional inorganic semiconductor devices. For example, thin interlayers of PTCDA significantly modify the device characteristics of GaAs Schottky diodes [18]. PES was used to determine the energy level alignment of PTCDA interfaces with several GaAs surfaces and it was found that the band line-up is very sensitive to the substrate preparation [19]. This is not consistent with the simple vacuum level alignment rule and implies the presence of an interface dipole at each interface. PES was also used to determine the energy level alignment for CuPc films grown on semiconductor surfaces [20,21] and fluorinated Pcs on metals [22,23]. Similar to the perylene case, the energy level alignment is influenced by the substrate treatment and morphology.

Even though perylene derivatives and Pcs have been studied quite extensively by means of optical methods, the direct and inverse PES combination was hardly employed for their characterization. IPES was employed to characterize for example CuPc and H_2Pc absorbed on Ag and Cu [24]. Comparing the results to MO calculations a symmetry assignment of the unoccupied π^* orbitals of these molecules was achieved. A series of 3D-transition metal Pcs were investigated by means of IPES by Yoshida et al. [25]. Similar IPES spectra were obtained for H_2Pc and CuPc. A minor contribution of the metal to the spectra was observed due to the dominant emission from the macrocyclic π orbitals of the Pc framework. However, there are several representative examples from literature where the transport gap (HOMO–LUMO separation) was determined in this manner. Hill et al. [26] performed combined photoemission and inverse photoemission measurements on thin PTCDA and CuPc films [26]. Taking into account polarization effects at the surface and in the bulk of the organic film they estimated their transport gaps to be (3.2 ± 0.4) eV and (2.3 ± 0.4) eV, respectively. Gao and Kahn [27] determined in a similar way the transport gap of (1.95 ± 0.4) eV for ZnPc [27]. This will be discussed further in the following sections.

This review focuses on energy level alignment at inorganic/organic interfaces and the transport energy gaps measured via direct and inverse photoemission spectroscopy, which are relevant for carrier injection and transport through two classes of the organic materials; i.e. perylene derivatives and phthalocyanines. The outline of this paper is as follows: Section 2 addresses the terminology of the transport gap and optical gap in organic materials followed by a short overview and comparison with other results. These results are then discussed in comparison with those obtained by two independent methods that allow the LUMO position to be determined. We will discuss in more detail the determination of the energetic positions and gaps via direct photoemission and inverse photoemission taking into account the widths of the HOMO and LUMO features in molecular solids and justify the approach of edge-to-edge distance for deriving the band gap. In the following section the transport gap determined by combining direct and inverse PES for three different perylene derivatives are presented. The results are then discussed in comparison with those from Section 2. They underline the proposition that the transport gap can be estimated very well from the edge positions of the HOMO and LUMO features after a proper deconvolution using the instrumental broadening. The concepts developed in the previous sections are then applied to the phthalocyanines. For both classes of materials the experimentally determined values for the transport gap are compared with the optical gaps. Similarities and differences will be highlighted. We close this review with a summary of the experimental results.

2. Transport gap and optical gap in organic materials

The energy separation between HOMO and LUMO in an organic solid is called HOMO–LUMO gap. The charge injection processes requires promotion of an electron or a

hole from the electrodes into one of the charge transport (HOMO or LUMO) states of the organic film. In organic semiconductors the charge carrier states are highly localized on individual organic molecules. Several factors contribute to this localization. First there is the small overlap between wave functions that lead to bandwidths of the HOMO and LUMO levels up to typically 200 meV. In energy bands being very narrow conduction occurs via tunneling and hopping between molecular sites justifying the modest mobilities. The second localizing phenomenon is the polaron formation driven by the electron–phonon interaction which is in particular effective in organic solids having both strongly coupled intramolecular phonons and many low energy intermolecular modes. Consequently, a simple addition or removal of a charged particle will induce polarization effects. The transport gap, E_t, which is the energy necessary to create a separated electron–hole pair, thus has a substantial polarization energy contribution (1–2 eV). Still it exceeds the optical gap, E_{opt}, by ~1 eV. The optical gap corresponds to the formation of a Frenkel exciton with the electron and hole on the same molecule or a Change Transfer exciton with the electron and hole on two adjacent molecules. The calculated difference between E_t and E_{opt} should be close to the exciton binding energy which can be as large as 1 eV [26]. This difference between optical and transport gap is usually ignored for inorganic semiconductors due to the low Wannier exciton binding energy. For inorganic semiconductor the band gap can thus often be obtained from the onset of the optical absorption spectra and E_t equals in a good approximation the optical gap, E_{opt}.

Considering excitons in organic materials measurements employing electron energy loss provided an interesting correlation between the length of molecule and the size the exciton [28]. It was reported that in conjugated polymers the exciton binding energy is small (~200 meV) while in small molecules like C_{60} the exciton binding energy is larger than 1.5 eV. However, the issue of the exciton binding energy continues to be a controversial one. Detailed experimental information on the exciton properties, in particular their dispersion, is not available to date despite the tremendous importance of such data as a basis for a complete understanding of the various phenomena in organic molecular solids.

Here direct Valence Band PhotoEmission Spectroscopy (VB-PES) combined with inverse photoemission spectroscopy (IPES) were used to probe the transport gap (E_t), while UV–vis and spectroscopic ellipsometry measurements were used to investigate the optical gap (E_{opt}). Moreover, combined VB-PES and IPES is the equivalent of an experiment in which the electron is removed from the molecule (VB-PES) or added to the molecule (IPES). Comparison of the energy difference between the hole induced state and electron induced state with the energy of formation of a electron–hole pair (E_{opt}) leads to an approximation of the exciton binding energy. Beyond the evaluation of the exciton binding energy, the main interest in this review is to provide an accurate determination of the transport gap in organic molecular solids. This requires consideration of several points.

First, for organic semiconductors the molecular polarization and charge localization complicates the situation. When a charge carrier is brought into a molecular solid, its field polarizes the surrounding molecules. A secondary polarization field created by polarized molecules contributes to the total self-consistent polarization clouds that surround each charged particle. The formation of these polarization clouds is associated with the stabilization energy P^+ for cations and P^- for the anions. Since Coulomb interactions are long-ranged, polarization clouds can extend over many lattice constants and P is significantly different at a free surface, near a metal–organic interface, in thin organic layers and in the bulk [29,30]. The second point that is related to the first is that VB-PES and IPES are surface sensitive techniques and as such provide about electron states located predominantly in the surface molecules.

As already mentioned above combined direct-inverse PES measurements were so far only performed on thin PTCDA and CuPc films by Hill et al. [26] and Gao and Kahn [27] on thin films of ZnPc. In Hill's work the HOMO–LUMO separation for PTCDA, as measured by the *peak-to-peak* distance, is (4.0 ± 0.1) eV. This value is assumed to be the distance between the centroids of the two peaks representing the HOMO and LUMO of a single molecule. However, this value suffers corrections related to the width of the observed peaks. The first correction is due to vibrational excitations that tend to shift both the measured HOMO and LUMO peaks away from the Fermi level. Therefore, the measured peak-to-peak separation increases by the Franck–Condon maxima which are estimated to be about 100 meV for each peak [31]. The next correction is attributed to the above mentioned difference between bulk and surface polarization. The correction to obtain the bulk from the surface polarization was first experimentally estimated by Salaneck to be around 0.3 eV for a molecule like anthracene [32] and theoretical methods to estimate the polarization energy in the bulk were developed by Soos et al. [33]. Consequently, the correction from measured HOMO–LUMO gap to the bulk E_t is obtained by adding the charge separation energy of 0.3 eV for the HOMO and 0.3 eV for the LUMO and the total correction is summing up to 0.8 eV. Finally, the transport gap of PTCDA estimated by Hill et al. [26] is (3.2 ± 0.4) eV.

Electrical transport measurements such as current–voltage (J–V) characteristics can provide further hints on the widths of the transport gap. Results obtained in our group revealed that the effective barrier height of Ag/PTCDA/GaAs(100) Schottky contacts changes as a function of GaAs(100) surface pre-treatment and as a function thickness of the PTCDA interlayer. Crucial for the understanding of J–V characteristics of the organic modified diode is the energy level alignment. Since the substrates used and

the organic material are primarily electron conducting, the barrier for electrons is determined by the offset between the conduction band minimum (CBM) and LUMO. Particular the position of the latter is usually not well known.

Fig. 1 shows the in situ J–V characteristics of an organic modified Ag/S-GaAs(100) and Ag/GaAs(100) Schottky contact on a semi-logarithmic scale. For S-passivated GaAs(100) substrates the barrier height is found to increase for thin PTCDA layers, ~5 nm. On the other hand, the J–V measurements for GaAs(100) substrates cleaned by hydrogen plasma reveal that the barrier height is found to decrease for thin PTCDA layers, ~6 nm. An increase in the barrier height for Ag/PTCDA/S-GaAs(100) contacts indicates that the electrons have to overcome an additional barrier. This additional barrier is due to the CBM–LUMO offset and indicates that the E_{LUMO} position is above E_{CBM}. The distance between E_{LUMO} and E_{CBM} can be estimated by the increase in barrier height to be approximately 0.13 eV. A decrease in barrier height for Ag/PTCDA/GaAs(100) contacts, on the other hand, indicates that E_{LUMO} is at or below E_{CBM}. The HOMO–LUMO transport gap of PTCDA can then be estimated to be 2.51–2.54 eV using the energy level alignment determined by VB-PES shown on the right side of Fig. 1. Using VB-PES only the offset between the Valence Band Minimum (VBM) and the HOMO can be determined. The transport gap results from adding the band gap of GaAs and the additional barrier determined from the J–V measurements.

Besides in situ J–V characteristics there is another independent method developed to evaluate the LUMO position. It employs the interface dipole at interfaces between PTCDA or DiMe-PTCDI and differently treated GaAs(100) surfaces [11,19,34]. It was proposed that for a vanishing interface dipole the CBM and the LUMO align, or, in other words, the electron affinity of the organic semiconductor equals the electron affinity of the GaAs substrate. A strong correlation is found between the interface dipole and the relative energy position of E_{LUMO} and E_{CBM}, respectively, the electron affinities of PTCDA or DiMe-PTCDI (EA_O) and the substrate (EA_{GaAs}). E_{HOMO} is always located well below E_{VBM}. A detailed description of the interface dipole formation at the interfaces between PTCDA/n-type GaAs and DiMe-PTCDI/n-type GaAs was given elsewhere [11,19] and is not discussed in detail in this work. However, the basic idea is that at thermal equilibrium, the number of electrons and holes that are transported across the interfaces should be equal. Due to the difference in EA and IE between the substrate surfaces and the organic films, each electron and hole transported undergoes an energy loss or gain. The net energy loss, therefore, depends on the electron and hole concentration that is transported across the interface and the energy difference of $EA_{GaAs} - EA_O$ and $IE_{GaAs} - IE_O$. The interface dipole is formed in order to compensate the net energy loss. Since the GaAs used as substrate is doped for n-type conduction, it is expected that the number of electrons transported across the interface with the organic film is much higher than that of holes and, therefore, $EA_{GaAs} - EA_O$ can be proposed to be the driving force for the interface dipole formation.

In Fig. 2 the interface dipole is presented as a function of EA_{GaAs}. It can be seen that the interface dipole formed at the organic/GaAs(100) interfaces is linearly dependent on

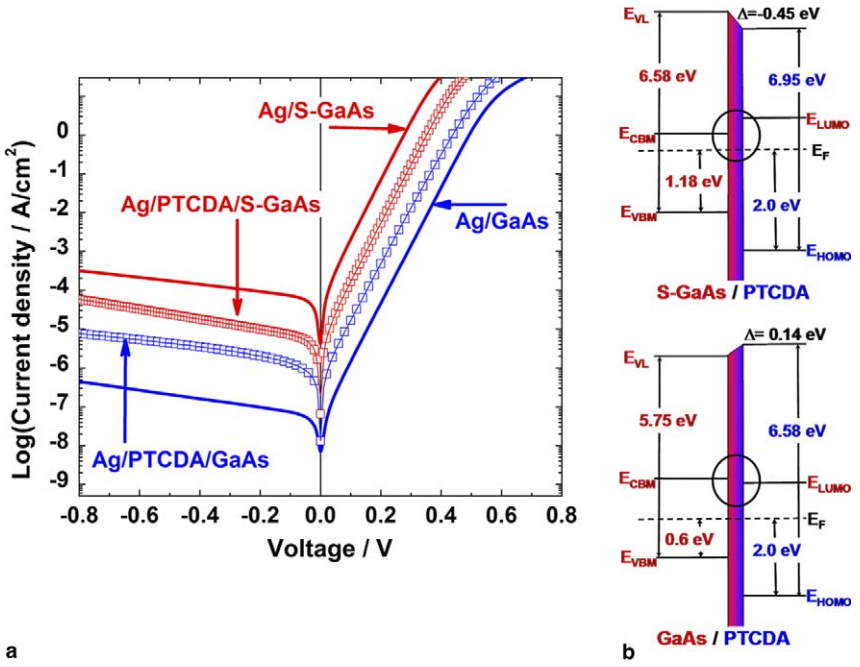

Fig. 1. (a) In situ J–V characteristics of Ag/GaAs(100), Ag/S-GaAs(100) (solid lines), Ag/PTCDA(6 nm)/GaAs(100) and Ag/PTCDA(5 nm)/S-GaAs(100) Schottky contacts (circles) shown on a semi-logarithmic scale. (b) Energy level diagram for PTCDA/S-GaAs(100) and PTCDA/GaAs(100) interfaces measured my means of VB-PES.

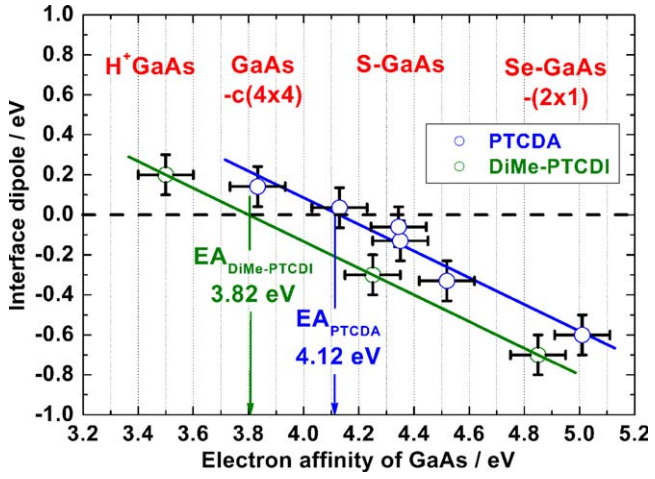

Fig. 2. The interface dipole formed at PTCDA/GaAs(100) and DiMe-PTCDI/GaAs(100) interfaces versus electron affinity of GaAs(100).

EA_{GaAs}. Using a linear fit, the interface dipole for PTCDA is found to be zero at $EA_{GaAs} = (4.12 \pm 0.10)$ eV. This value also represents EA_{PTCDA} assuming that the formation of the interface dipole is driven by the difference between the electron affinities. For DiMe-PTCDI, on the other hand, EA_{GaAs} was found to be zero at (3.82 ± 0.10) eV. With the ionization energies of $IE_{PTCDA} = (6.95 \pm 0.08)$ and $IE_{DiMe\text{-}PTCDI} = (6.6 \pm 0.15)$ eV, a transport gap of (2.83 ± 0.1) eV for PTCDA and of (2.78 ± 0.1) for DiMe-PTCDI is determined.

Therefore, from in situ J–V characteristics and the interface dipole cancellation method values in the range of 2.51–2.83 eV for the transport band gap of PTCDA are expected. These are significantly smaller than the value for the transport gap of PTCDA proposed by Hill et al. [26].

Besides the methods presented above another method that was employed to determine the transport gap of organic materials is cyclic voltammetry. It was used to determine the reduction and oxidation potentials (redox potentials) of metallophthalocyanines in solution. The first redox potentials correspond to the removal or addition of one electron and the summation of these potentials should thus provide values related to the transport gap of the materials. The potentials were measured, among other metallophthalocynines, for H_2Pc [35,36] and CuPc [35]. The transport gap determined in this way is 1.76 eV/2.0 eV for H_2Pc and 1.76 eV for CuPc. In the CuPc case the value is smaller than that proposed by Hill et al. [26]. Electrical measurements of the charge injection process with electrochemical methods where ions are created and/or counter charge are solved in an electrolyte are equilibrium processes where the system has sufficient time to fully "adjust" to the new charge distribution. Thus the situation is not comparable to the solid state case and care has to be taken when using values determined from electrochemistry e.g. for predicting energy level alignments.

As argued above, the transport gap of organic molecular solids cannot be determined by means of optical spectroscopies (or cyclic voltammetry) and requires the VB-PES-IPES combination. Moreover, the *peak-to-peak* method used to determine the transport gap seems to overestimate its value.

3. Experimental and data analysis

The experiments described in this review focus exclusively on organic molecular beam deposited thin films of π-conjugated molecules.

The perylene derivatives, PTCDA, DiMe-PTCDI and PTCDI were purchased from Sensient Imaging Technologies GmbH (former SynTecGmbH, further being purified twice by sublimation at 575 K under high vacuum ($\sim 10^{-6}$ mbar). Each material was then filled into a quartz crucible that was mounted in a Knudsen cell-type evaporator. Before the evaporation of the organic material, the Knudsen cell was thoroughly degassed for a few hours at 200 °C. Organic thin films were prepared using organic molecular beam deposition (OMBD) from the Knudsen cells operating at 280 °C for all three organic materials. Sublimed CuPc and H_2Pc provided by Sensient Imaging Technologies GmbH were employed without further purification. F_4CuPc and $F_{16}CuPc$ were supplied by IAPC (University of Bremen). The Pcs were evaporated from Knudsen cells kept in a temperature range of 340–370 °C. For perylene derivatives the substrates were tellurium doped n-GaAs(100) (Freiberger Compound Materials GmbH, $N_D = 2 \times 10^{17}$ cm^{-3}). Prior to OMBD they were sulphur passivated. Details about the passivation can be found elsewhere [37]. During the deposition the substrates were kept at room temperature. The organic films were deposited at a rate of typically 0.2 nm/min up to a total thickness of 15 nm. For Pcs hydrogen passivated p-type, (111) oriented silicon with a doping concentration of approximately 1.5×10^{15} cm^{-3} served as substrate. The passivation process consists of a wet chemical etching in a solution containing HF (40%). After the passivation process the samples were transferred into UHV. The evaporation rates were in the range of 0.1 up to 2 nm/min with the substrate kept at room temperature. Evaporation rates and film thicknesses were monitored by means of a quartz crystal microbalance and confirmed by post-growth ellipsometry measurements. The thicknesses of the organic layers were always kept in a range (typically $\leqslant$20 nm) for which charging effects during the VB-PES and IPES experiments are negligible.

The principal techniques used in this work are valence band photoemission spectroscopy (VB-PES) and inverse photoemission spectroscopy (IPES). VB-PES is used to investigate the occupied electronic states of organic and inorganic materials below the Fermi level. A typical VB-PES spectrum of an organic thin film is shown on the left side of Fig. 3. It consists of a number of well defined features related to the density of occupied states of the molecular solid and a low energy secondary electron peak which results from inelastically scattered electrons. E_{HOMO} corre-

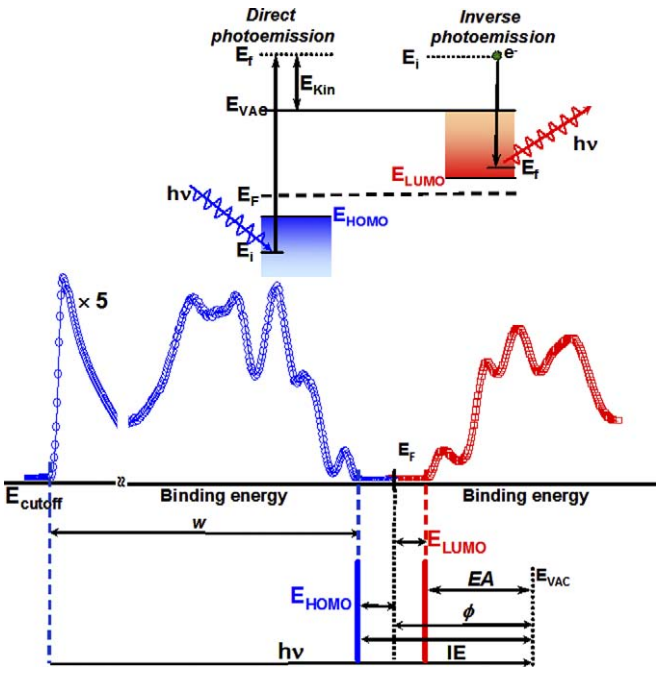

Fig. 3. A VB-PES and IPES spectra of a thin organic film from the HOMO to the low energy cutoff on the left side and unoccupied states with the LUMO on the right side.

sponds to the edge of the HOMO peak towards lower binding energy as measured with respect to the Fermi level. The ionization energy (IE) is measured by subtracting the total width of the spectra measured from the low kinetic energy onset to E_{HOMO} from the photon energy. The position of the vacuum level E_{VAC} is determined from the low kinetic energy edge of the secondary electron peak when a bias of -10 V is applied on the sample. A shift in the photoemission cutoff upon formation of an interface provides information on the interface dipole between the two materials. The energy resolution is about 80 meV when using synchrotron radiation and 150 meV when using a He I discharge lamp. For the UPS spectra no deconvolution of the instrumental broadening was performed since the instrumental resolution is much smaller than the width of the spectral features.

Using the time reversed photoemission process, inverse photoemission spectroscopy (IPES) provides information on the unoccupied electronic states in the energy region above the Fermi level. An electron with well-defined kinetic energy E_{Kin} impinges on the sample and couples to states in the solid which are lying above the vacuum level E_{vac} of the sample. From this initial state with energy E_i the electron decays radiatively to lower lying unoccupied electronic final states with energy E_f. In the IPES experiment the densities of unoccupied states are determined by sweeping the electron energy and keeping the energy of detected photons constant, i.e. in the isochromat mode. The IPES experimental set-up working in the isochromat mode is a "home" built system. The fixed-energy photon detector [38] consists of a Geiger–Müller tube with a magnesium fluoride (MgF_2) window filled with a gas mixture containing ethanol and argon. The ionisation energy of ethanol and the transmission function of the MgF_2 provide a value of 10.9 eV as the nominal detection energy of the detector. A low energy electron gun [39] was used to produce a mono-energetic electron beam. The overall IPES instrumental resolution as estimated from the width of the Fermi edge measured on an Ar sputtered nickel sample is 0.4 eV. Spectra were recorded at normal incidence with a current density in the range of 10^{-6} A/cm^2. This value is low enough in order not to damage the organic films. A typical spectrum (see right side in Fig. 3) has its onset above the Fermi level E_F and E_{LUMO} corresponds to the edge of the LUMO peak towards lower binding energy.

Due to the rather poor instrumental resolution of the IPES spectra a special treatment was required. It consists of a deconvolution of the spectra using a Gaussian function with a full width at half maximum (FWHM) of 0.4 eV. The LUMO edge determination for the PTCDA case is illustrated in Fig. 4. First the background in the IPES spectrum of 15 nm PTCDA deposited on sulphur passivated GaAs(1 0 0) is subtracted. The background used in this case is described by a cubic polynomial function, others such as exponential function were also considered. The choice of the background, however, has negligible influence on the LUMO energy position. The IPES data were then fitted using Gaussian peaks using a nonlinear least-squares fitting technique. The fitted peaks were then deconvoluted using Gaussian functions with a FWHM of 0.4 eV.

The contribution of these individual peaks to the overall intensity of the measured IPES data is plotted with thick lines and the deconvoluted contributions are plotted with open circles. As we shall see later from the theoretical cal-

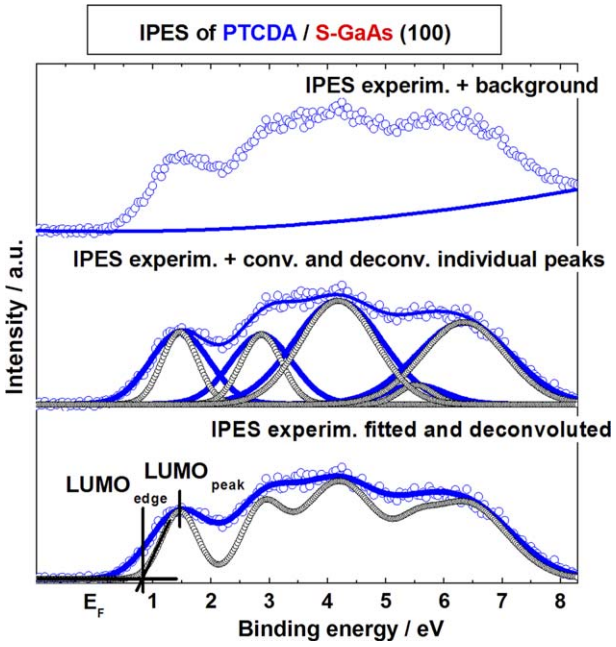

Fig. 4. The IPES spectra of a PTCDA thin film together with convoluted and deconvoluted individual peaks that contribute to the overall intensity.

culations the LUMO state is well separated, ~1.5 eV, from the other contributions to the density of the unoccupied states. However, its FWHM after deconvolution is larger than the FWHM of the HOMO by about ~0.2 eV. This is an inherent property of IPES spectroscopy and is related to the lifetime of the final states [40].

Consequently, the information on the electronic properties that can be derived from the combination of direct and inverse photoemission measurements is:

- The position of the highest occupied molecular orbital (HOMO), the ionization energy, the work function of the organic semiconductor, and the vacuum level position.
- The position of the lowest unoccupied molecular orbital (LUMO) of the organic semiconductor and the electron affinity as the difference between the vacuum level and the position of the LUMO.

Nevertheless, the HOMO and LUMO require special attention when evaluating their positions on the energy scale. In that respect it is useful to briefly reconsider the inorganic semiconductor case and refer for the moment just to the valence states. Nowadays accurate determination of valence band maxima (VBM) for inorganic semiconductors is essential for determining the effectiveness of band offset engineering at heterojunctions. In order to determine the valence band offset of a semiconductor heterojunction, detailed knowledge of the energy positions of the VBM of two adjacent materials is necessary. Due to the strong dispersion of the uppermost valence band VBM has to be determined at the correct point in k-space. This can be conducted by selecting suitable excitation energies and by employing a linear extrapolation of the VB edge [41]. This approach is experimentally justified by the excellent results obtained when using VB-PES and IPES to derive band edges for band gap determination [42]. The arguments which suggest that the linear extrapolation is the best approximation are: firstly, a limited angular resolution leads to a non-symmetric broadening towards higher binding energies due to the downward dispersion from the VBM in all k-directions. Secondly, inelastic scattering processes (such as phonon excitation) will also lead to a broadening which is more pronounced towards higher binding energies, because at room temperature an energy loss is more probable than an energy gain by such scattering processes. Thirdly, due to the fact that photoemission probes the final state of the system with the presence of a core hole screening processes play an important role. Incomplete screening on the timescale of the photoemission process leads to a spectral shift towards higher binding energies. Hence, if the screening is spatially and/or temporally inhomogeneous, it is the spectral weight with lowest binding energy, which most closely approximates the ground state. In summary, the discussed processes all lead to non-symmetric broadening towards higher binding energies, and in all three cases the spectral weight with lowest binding energy corresponds to the best approximation of the ground state properties.

In organic semiconductors the above discussed processes are also present. Moreover, due to charge localization the electron–phonon interaction is in particular effective in organic solids having both strongly coupled intramolecular phonons and many low energy intermolecular modes. Spatial variations in the electronic contributions to the intermolecular relaxation energies in the vicinity of the surface and local site-to-site variations in ion state energies due to the non-equivalent local environments in the non-single crystalline film can contribute to broadening as well. As mentioned in the introduction, the VB-PES spectrum will show the HOMO shifted by the polarization energy (P^+) induced by the presence of a molecular cation. Similarly the IPES spectrum shows the LUMO shifted by the polarization P^- induced by the presence of the molecular anion. Therefore, when analyzing the VB-PES and IPES features, the positions corresponding to HOMO and LUMO, respectively, are better represented by the edges of these peaks after a proper deconvolution with the instrumental broadening.

A comparison between the occupied and unoccupied electronic states measured via PES/IPES and those derived from density functional theory (DFT) [43] represent one good approach for providing fruitful information about the electronic structure. In this work the density of states (DOS) is simulated using molecular orbital calculations. These calculations were performed using the Gaussian'98 package [44] with the B3LYP method and 6-31++G(d,p) basis set to describe the core orbitals and the inner and outer part of the valence orbitals. Geometric structures of the molecules involved in this work were determined by performing optimization with the standard gradient technique in the same Gaussian'98 package. The calculated binding energies of each molecular orbital (MO) state for a single molecule are convoluted using Gaussian functions with a FWHM adapted to the experimental linewidths. No photoionization cross-section is included in the calculations. The calculated spectrum is then rigidly shifted in order to match the HOMO energy with the first experimental peak. However, a comparison between the energy scales is found not to be required to achieve a good match between the experimental and theoretical lineshapes [27,45]. Even though the origin of the difference is not easily understood, it is consistent with the fact that the methods, i.e. HF, B3LYP, etc. of the Gaussian'98 package, systematically overestimate the band gap of materials and with it the energy positions. On the basis of the B3LYP method results, the LCAO (linear combinations of atomic orbitals) patterns of occupied and unoccupied levels of the molecules involved in this work have been plotted and are discussed in the following sections.

For evaluating the exciton binding energy optical spectroscopies were employed. UV/VIS transmittance spectra were taken for all perylenes on quartz using a Specord M40 spectrometer. For phthalocyanines spectroscopic

ellipsometry measurements were performed using a variable angle spectroscopic ellipsometer (VASE by J.A. Woollam Co. Inc.) equipped with an auto-retarder and a Xe-lamp source.

4. Transport gap of perylene derivatives

The perylene derivatives, here 3,4,9,10-perylenetetracarboxylic dianhydride (PTCDA), 3,4,9,10-perylenetetracarboxylic-diimide (PTCDI), and *N*-*N*′-dimethyl-3,4,9,10-perylenetetracarboxylic diimide (DiMe-PTCDI) are organic semiconductors with a π-conjugated electron systems. When used as active elements in organic electronics the performance of devices depends on the efficiency of the charge transport. The charge transport properties are strongly depending on the molecular packing. Specific arrangements can lead to an increase of electron mobilities. Perylene derivatives form crystal structures with displaced dimers that arrange themselves in a herringbone fashion. Moreover, when the molecules are chemically tailored or modified major variations in solid state packing and electronic properties were observed. These modifications were discussed earlier by Klebe et al. [46] and are referred to as the crystalochromic effect. The possibility of changing the solid state packing by changing the individual molecules implies that the perylene derivatives can be used to tune the transport properties. At the same time the electronic properties can be considerably affected by the chemical modification (derivatization). Employing the VB-PES/IPES combination the effect of the functional groups (electron-withdrawing groups) on the HOMO and LUMO positions can be evaluated.

Moreover, insight into the electronic structure of the organic solids can be obtained by comparing measured and calculated densities of states. The calculated DOOS of PTCDA as shown in Fig. 5 (left) is similar with what was measured experimentally using a photon energy of 45 eV. This excitation energy was chosen based on photoionization cross-section considerations. In order to compare the simulated DOOS and the measured valence band spectrum the energy scale of the calculated spectrum was shifted by 0.65 eV towards higher binding energies. The calculated DOUS was obtained by Gaussian broadening of each orbital energy with a FWHM of 0.70 eV. In order to compare the simulated DOUS with the measured IPES spectrum the energy scale of the calculated spectrum was shifted by 0.87 eV towards the Fermi level. The value of the Gaussian FWHM was taken equal to the FWHM of the experimentally deconvoluted LUMO state. The vertical bars in this figure represent the calculated binding energies of each molecular orbital (MO) state for a single molecule.

Even though there is a common drawback for all approaches based on DFT in predicting the energy gap, the trends in calculated values were found satisfactory in understanding some physical phenomena. As shown in Fig. 5, the agreement between the experimental and theoretical lineshapes is very good. The highest occupied and lowest unoccupied molecular orbital, respectively, originate from a single molecular orbital with π character which is distributed predominantly over the perylene core. The good agreement demonstrates that the electronic properties of organic molecular films are still close to those of the individual molecule.

VB-PES and IPES measurements of 15 nm PTCDA, DiMe-PTCDI and PTCDI films deposited onto sulphur passivated GaAs(100) are presented in Figs. 6–8. The VB-PES data are depicted on the left side of the figures, while the IPES data are on the right side. Contributions

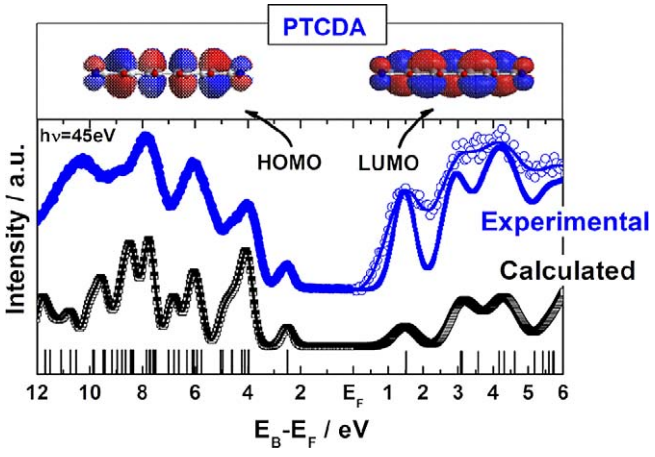

Fig. 5. VB-PES and IPES spectra of a thick PTCDA layer compared to the calculated molecular orbitals (MO) of a single molecule. The calculated spectra are the result of the convolution of Gaussian functions centered on the MO and having a FWHM determined from the fit of the experimental HOMO and LUMO features.

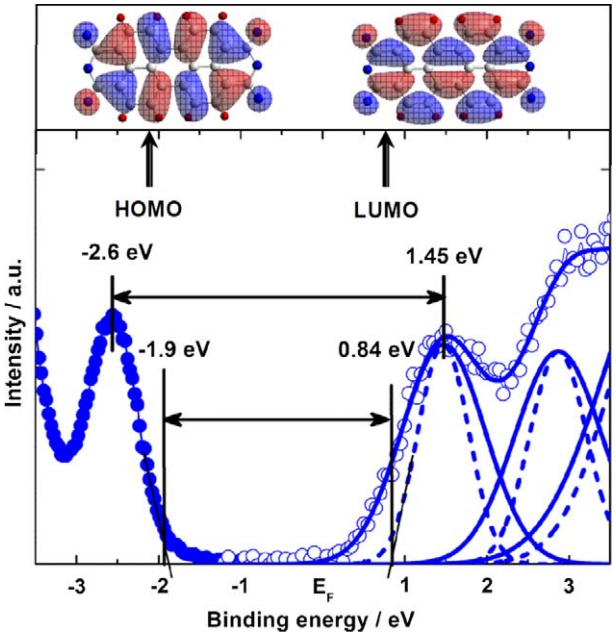

Fig. 6. Combined VB-PES and IPES measurements of PTCDA with the charge density contours of the HOMO and LUMO on top of the figure.

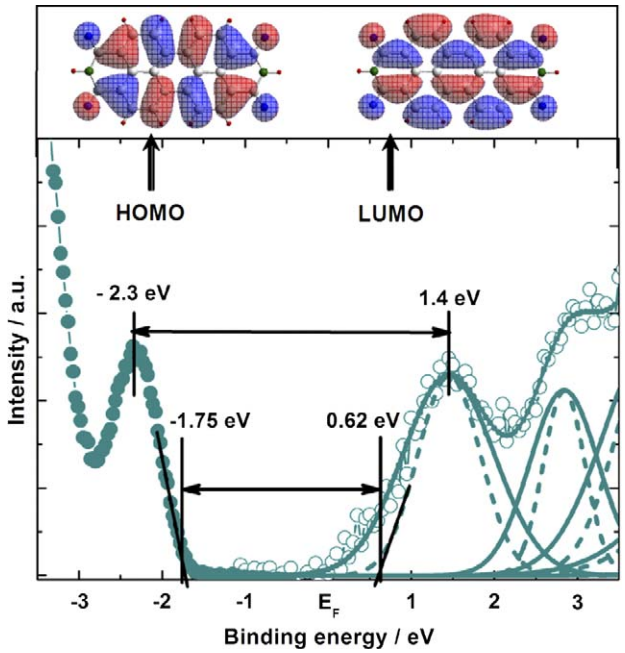

Fig. 7. Combined VB-PES and IPES measurements of PTCDI with the charge density contours of the HOMO and LUMO on top of the figure.

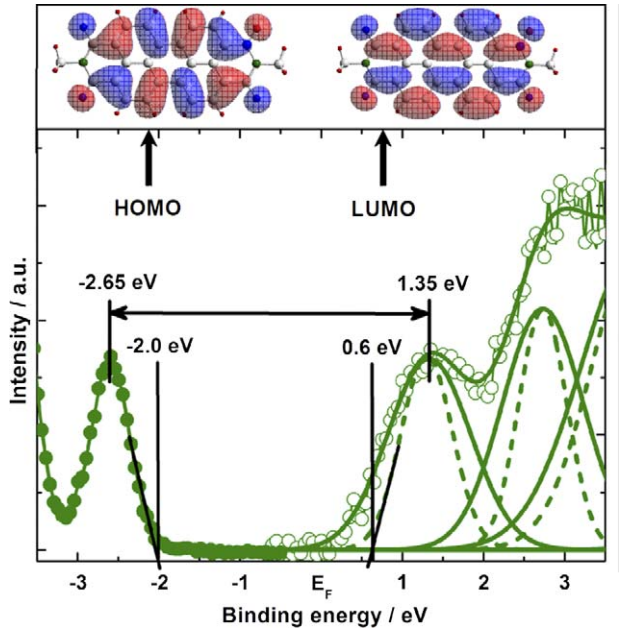

Fig. 8. Combined VB-PES and IPES measurements of DiMe-PTCDI with the charge density contours of the HOMO and LUMO on top of the figure.

of the individual peaks to the overall intensities of the experimentally measured IPES data are plotted with lines while the deconvoluted contributions are plotted with dashed lines. The VB-PES and IPES spectra for all the perylene derivatives were aligned on the energy scale with respect to the Fermi level.

The HOMO and LUMO energy positions (edges) are determined from the intercept of two linear extrapolations.

Table 1
Transport gap of PTCDA, DiMe-PTCDI and PTCDI as determined from combined measurements of VB-PES and IPES

	$(E_{\text{Transport}}^{\text{edge-to-edge}} \pm 0.2)$ (eV)	$(E^{\text{peak-to-peak}} \pm 0.2)$ (eV)	E_{Optical} (eV)
PTCDA	2.74	4.05	2.22
DiMe-PTCDI	2.6	4	2.16
PTCDI	2.37	3.7	2.17

For comparison the optical gap values obtained from the spectra in Fig. 9 are presented as well.

One is describing the background and the second one being a tangent to the most prominent band edge in the inflection point. However, for comparison purposes with the literature data the peak-to-peak energy is shown as well. The results obtained for the three perylene derivatives are given in Table 1. The resulting transport gaps show a dependence on the functional groups. The addition of a more electronegative functional group to the perylene core leads to stabilization of both occupied and unoccupied energy levels. The replacement of the anhydride group by the less polar imide or methylimide group leads to a smaller energy splitting between the energy levels since the charge is moved from the aromatic part, acting like a donor, to the accepting functional groups. It seems that the electron-withdrawing groups strongly influence the energy positions, especially the LUMO levels. Moreover, it is noticeable that such chemical derivatization does not influence the shape of the molecular orbitals. As depicted above in Figs. 6–8 the charge densities related to the HOMOs and LUMOs are mainly distributed over the perylene core and have π-character. The trend observed for the transport gap is also preserved in the values for the optical gaps of these materials. These values were determined from the position of the first absorption peak in optical absorption (see Fig. 9).

It is now time to compare the VB-PES/IPES results with the results obtained using the interface dipole cancellation method. With the ionization energies presented in Fig. 10 a transport gap of (2.85 ± 0.1) eV for PTCDA and of

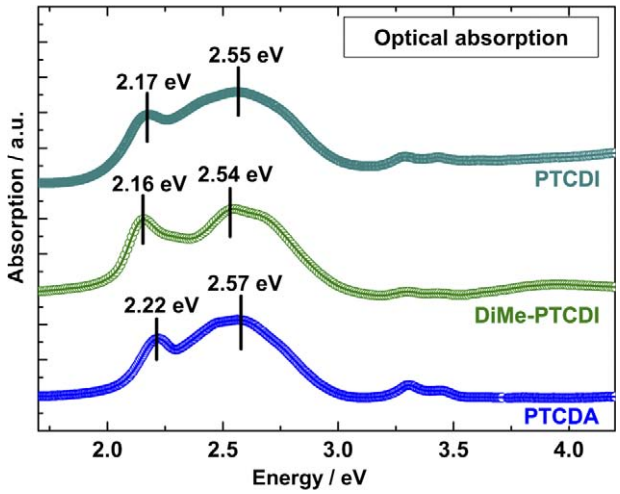

Fig. 9. Optical absorption spectra of PTCDA, DiMe-PTCDI and PTCDI.

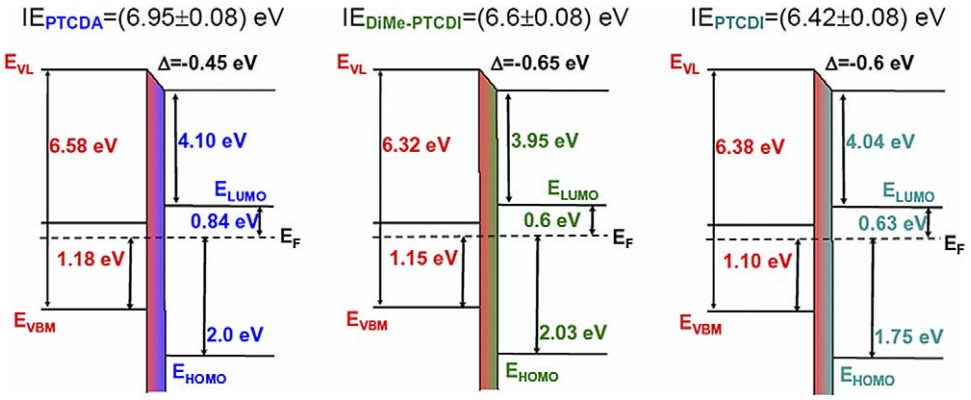

Fig. 10. Energy level alignment at the organic/S-GaAs(100) interfaces measured using VB-PES for determining the HOMO, ionization energy and work functions, and IPES for determining the LUMO position.

(2.65 ± 0.1) for DiMe-PTCDI was determined. The values of (4.1 ± 0.2) eV for EA_{PTCDA} and (3.95 ± 0.2) eV for $EA_{DiMe\text{-}PTCDI}$ are in very good agreement with the ones determined by $\Delta = f(EA)$, being (4.12 ± 0.1) eV for PTCDA and (3.82 ± 0.1) eV for DiMe-PTCDI. The value for the band gap of PTCDA is larger than the one expected from the *J–V* characteristics but taking into account the experimental error of ±0.2 eV for IPES all values are in good agreement. Consequently the *edge-to-edge* method for determining the transport gap is proposed to provide reliable values for the transport gap.

5. Transport gap of phthalocyanines

Although quite extensively studied materials, phthalocyanines were rarely evaluated using combined direct and inverse PES in order to determine the transport band gap, [26]. In particular, for the following Pcs: H_2Pc, F_4CuPc and $F_{16}CuPc$ involved in this work there are no known studies of their transport gap using VB-PES and IPES.

Fig. 11 displays a comparison of the VB-PES and IPES experimental spectra and calculated molecular orbitals (MO) of H_2Pc. The experimental spectra were recorded on layers of 20 nm thickness of H_2Pc. The calculated MO energy positions using Gaussian'98 are obtained with respect to the vacuum level. Their positions were scaled to the Fermi level by adding the experimentally determined work function of the organic material. On the left hand side of Fig. 11 the experimental and simulated VB-PES spectra are shown. The Gaussian functions used to generate the simulated spectra have a FWHM of 0.5 eV. The calculated positions of MO were shifted away from the Fermi level by 0.48 eV in order to fit the calculated HOMO with its experimentally determined position. On the right-hand side of Fig. 11 the experimental and simulated IPES spectra are shown. The experimental data are displayed together with the fit and the deconvoluted spectra. The FWHM of the deconvoluted LUMO (0.63 eV) was taken into account for the simulation of the calculated MO. The simulated spectra were shifted away from the Fermi level by approximately 0.65 eV for the calculated LUMO peak position to fit with experimental one. However, we have to note that the first peak in the IPES spectra is composed of two states as judged from the DFT calculation. In the upper panel of Fig. 11, we show the charge density contours of the HOMO and LUMO on the H_2Pc molecule. In the case of the density of unoccupied states the presented LUMO is the lowest energy occurring from the calculation. There is quite good agreement between the lineshapes of the simulated and experimental spectra and this proves again the weak inter-molecular interaction present in the organic layer.

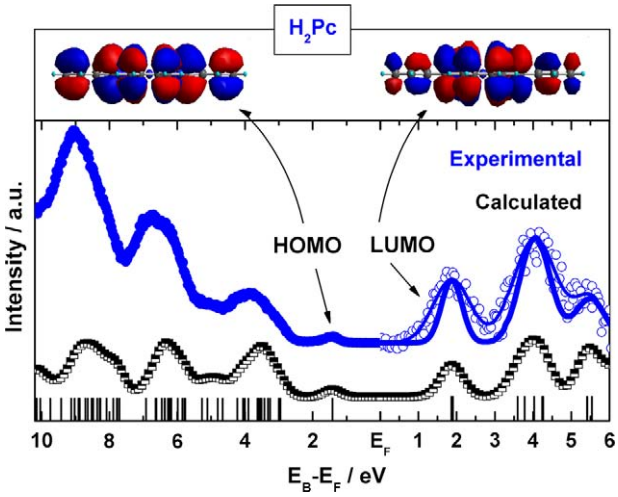

Fig. 11. VB-PES and IPES spectra of thick H_2Pc layer compared to the calculated molecular orbitals (MO) of a single H_2Pc molecule. The calculated spectra are the result of the convolution of Gaussian functions centred on the MO and having a FWHM determined from the fit of the experimental HOMO and LUMO features.

Fig. 12 shows a zoom in the HOMO–LUMO region for all four phthalocyanines. The VB-PES and IPES experimental data were scaled in order to be plotted in the same graph. In each case the HOMO position was determined by extrapolating the lower binding energy edge to the background. On the other hand, the LUMO was fitted and the resulting peak deconvoluted. The LUMO position

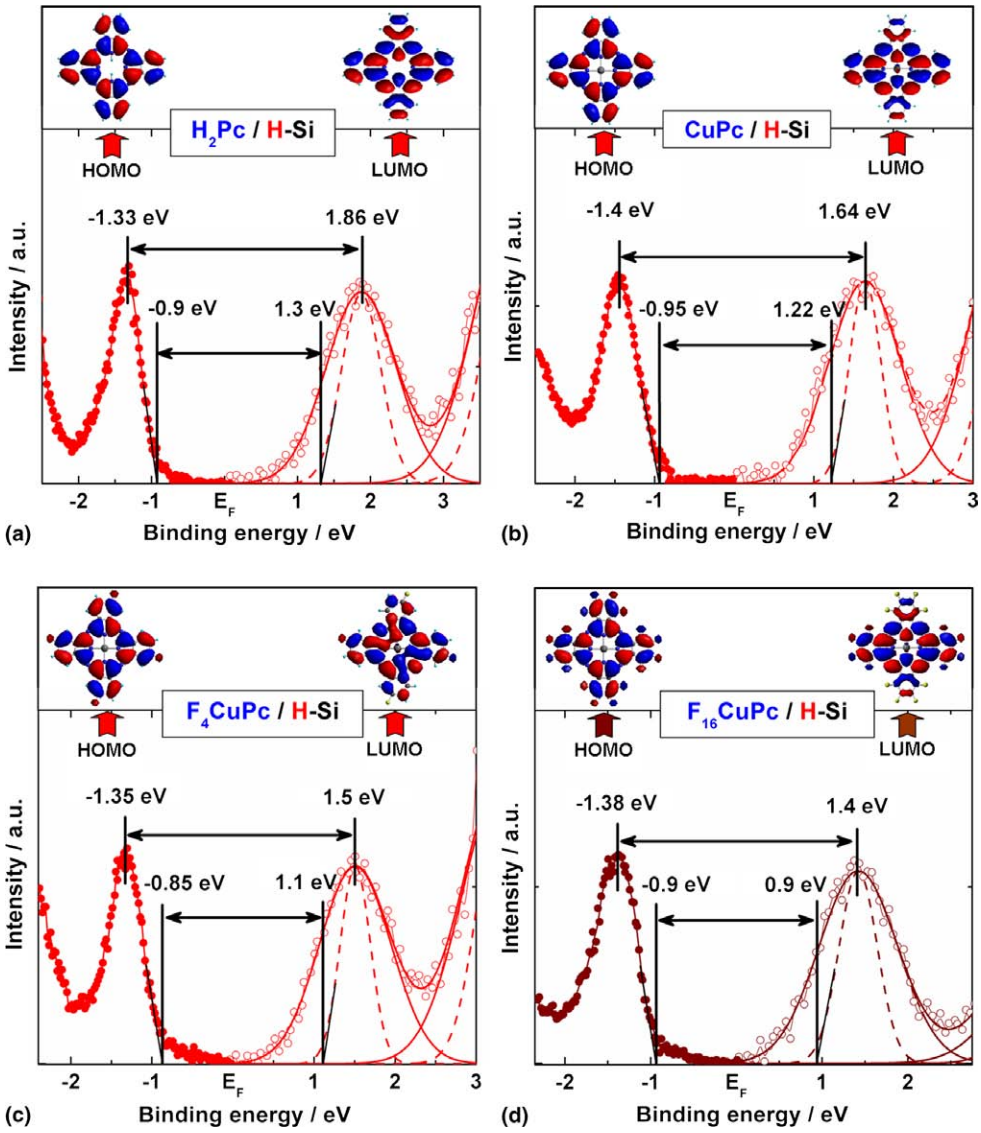

Fig. 12. Determination of the transport gap for: (a) H_2Pc, (b) CuPc, (c) F_4CuPc and (d) $F_{16}CuPc$.

was determined from the extrapolation of the lower binding energy edge of the peak obtained after deconvolution. The charge density contours of the HOMO and LUMO are included in the upper panel of each figure.

The energy band diagrams of the Pcs are displayed in Fig. 13. The hydrogen passivated silicon substrate is included as well. For simplicity the band bending of the substrate is omitted. The electronic properties of the H–Si surface are the following: $IE = (5.02 \pm 0.07)$ eV and $\Phi = (4.22 \pm 0.07)$. The electronic properties of all four Pcs are summarised in Table 2. When evaluating the obtained electronic properties of H_2Pc and CuPc, we observe slightly lower IE, Φ and EA values for CuPc than for H_2Pc. The difference amounts to approximately 0.15 eV. This is expected when taking into account the electron affinity of Cu (1.22 eV) [47,48] which is lower than the EA of H_2Pc. Thus the addition of a Cu atom to the H_2Pc molecule brings additional charge (valence electrons) and decreases the overall EA of the resulting molecule (CuPc). Then again, the addition of fluorine to the CuPc molecule increases EA as shown in Table 2 for the fluorinated Pcs. Considering that the EA of fluorine has a value of 3.2 eV, an overall increase in EA of a molecule is expected. Moreover, the change in interface dipoles is also driven by the change in EA. Thus the interface dipoles that arise at the interfaces scale linearly with the electron affinities of the Pcs. Fig. 14 shows a plot of the interface dipole formed at Pc/H–Si interfaces as a function of the EA of each Pc. The dashed line is the linear fit to the experimental data points. The slope of the linear fit is 0.75. Such a strong drop in the interface dipole due to fluorination was observed as well for the fluorinated Pcs deposited on Au [49]. A linear dependence of IE and Φ was also observed, but the calculated slope is around 1.

Similarly to the previously described electronic properties, the resulting transport gaps show a dependence on the degree of fluorination. In detail E_t of CuPc and H_2Pc has the same value of (2.2 ± 0.2) eV, then E_t decreases with

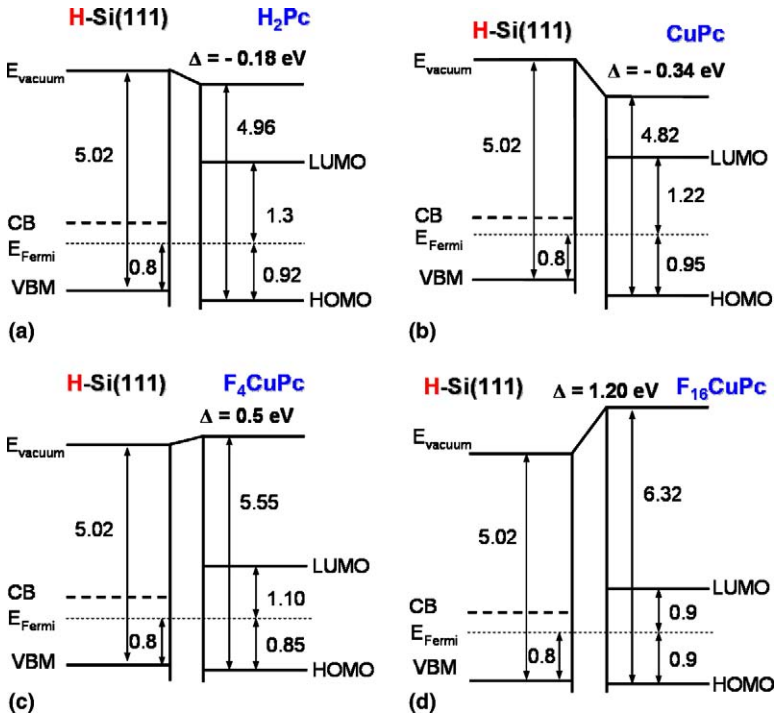

Fig. 13. Energy band diagrams of: (a) H_2Pc/H–Si, (b) CuPc/H–Si, (c) F_4CuPc/H–Si and (d) $F_{16}CuPc$/H–Si systems.

Table 2
Electronic properties of Pcs

	Φ (eV)	IE (eV)	EA (eV)
H_2Pc	(4.04 ± 0.07)	(4.96 ± 0.07)	(2.74 ± 0.2)
CuPc	(3.87 ± 0.07)	(4.82 ± 0.07)	(2.65 ± 0.2)
F_4CuPc	(4.70 ± 0.07)	(5.55 ± 0.07)	(3.60 ± 0.2)
$F_{16}CuPc$	(5.42 ± 0.07)	(6.32 ± 0.07)	(4.52 ± 0.2)

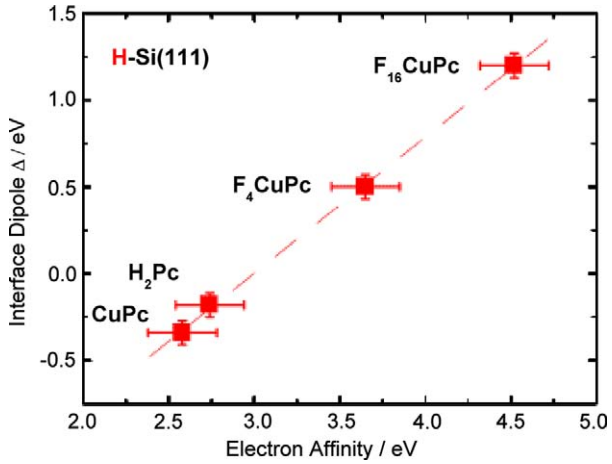

Fig. 14. Interface dipole formed at Pc/H–Si interfaces as a function of the electron affinities of the Pcs.

the increasing number of fluorine atoms in the molecule, e.g. (1.95 ± 0.2) eV for F_4CuPc and (1.8 ± 0.2) eV for $F_{16}CuPc$. This trend is also preserved in the values of the optical gaps of these materials. The presence of the same value for E_t of CuPc and H_2Pc is expected since there is no metal contribution to their HOMO and LUMO [25]. Fig. 15 shows the imaginary part of the dielectric function ε_2 for the Pcs/H–Si systems obtained from spectroscopic ellipsometry measurements [50–52]. In the energy range of 1.4 eV up to 2.4 eV the Q absorption band of Pcs resides [50]. The first absorption peak placed at lowest energy corresponds to the optical gap of the organic material. The values for the optical gaps as well as the values for the transport gaps are shown in Table 3.

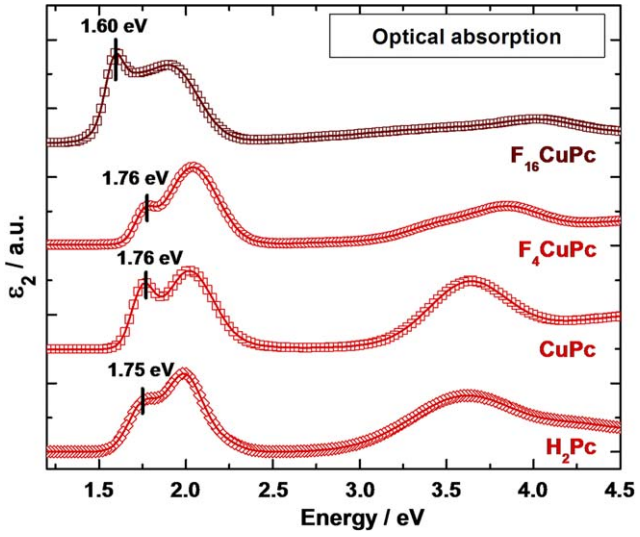

Fig. 15. Imaginary part of the dielectric function (ε_2) for H_2Pc, CuPc, F_4CuPc and $F_{16}CuPc$. The spectra were rescaled in order to be plotted in the same graph. Marked with vertical line are the first absorption peaks the positions of which correspond to the optical gaps.

Table 3
Transport gaps and optical gaps of phthalocyanines

	E_t (eV)	E_{opt} (eV)
H_2Pc	(2.2 ± 0.2)	1.75
CuPc	(2.2 ± 0.2)	1.76
F_4CuPc	(1.95 ± 0.2)	1.76
$F_{16}CuPc$	(1.8 ± 0.2)	1.60

In addition, the HOMO and LUMO of the fluorinated molecules are extended over the fluorine atoms. This clearly indicates that the fluorine modification of phthalocyanines plays the major part in the band gap, electron affinity (EA) and ionization energy (IE) changes. This can be analyzed based on the high electronegativity of the fluorine atoms. Fluorine having an electronegativity of 4 eV, the maximum value on the Pauling scale, induces additional charge of positive sign on the π system of the Pcs. Therefore, IE increases as a function of the number of fluorine atoms. However, when addressing the EA increase of the Pc molecules upon fluorine modification, the electron affinity of fluorine (EA_F) must be taken into account. The EA_F has a value of 3.2 eV resulting in a different slope of the increasing EA function. Thus the transport gap varies with the increasing number of fluorine atoms.

6. Summary

Using direct valence band photoemission spectroscopy and inverse photoemission spectroscopy the densities of occupied and unoccupied electronic states of perylene derivatives and phthalocyanines were investigated. It is proposed that the transport gap of organic materials can be obtained from the edge-to-edge distance between the HOMO and LUMO features. The resulting values of the transport gaps are in good agreement with results of electrical measurements and another method of deriving the transport gap employing measurements of the interface dipole at inorganic/organic interfaces. Still the error bar for the band gap values is too large and further improvement in the determination of the gap values is needed in order to make precise prediction of energy level alignment at interfaces involving organic semiconductors and thus heterostructure engineering possible.

Acknowledgements

This work was supported by the EU funded Human Potential Research Training Network DIODE (Contract No. HPRN-CT-1999-00164) and the BMBF (No. 05KS10CA/1, MUSTANG 05KS40C1/3). The authors like to thank Dr. W. Braun and Dr. D. Vyalikh for fruitful discussions and support and Prof. Dr. D. Schlettwein for providing the fluorinated phthalocyanine materials.

References

[1] R.H. Friend, R.W. Gymer, A.B. Holmes, J.H. Burroughes, R.N. Marks, C. Taliani, D.D.C. Bradley, D.A. Dos Santos, J.L. Bredas, M. Logdlund, W.R. Salaneck, Nature 397 (1999) 121.
[2] S.R. Forrest, Chem. Rev. 97 (1997) 1793.
[3] M. Baldo, M.E. Thompson, S.R. Forrest, Nature 403 (2000) 750.
[4] Y. Hirose, S.R. Forrest, A. Kahn, Phys. Rev. B 52 (1995) 14040.
[5] C.D. Dimitrakopoulos, P.R.L. Malefant, Adv. Mater. 14 (2002) 99.
[6] D.R.T. Zahn, T.U. Kampen, H. Méndez, Appl. Surf. Sci. 112–213 (2003) 423.
[7] T.U. Kampen, G.N. Gavrila, H. Méndez, D.R.T. Zahn, A.R. Vearey-Roberts, D.A. Evans, J. Wells, I. McGovern, W. Braun, J. Phys.: Condens. Mat. 15 (2003) S2679.
[8] D.A. Evans, H.J. Steiner, S. Evans, R. Middleton, T.S. Jones, S. Park, T.U. Kampen, D.R.T. Zahn, G. Cabailh, I.T. McGovern, J. Phys.: Condens. Mat. 15 (2003) S2729.
[9] Y. Hirose, A. Kahn, V. Aristov, P. Soukiassian, V. Bulovic, S.R. Forrest, Phys. Rev. B 54 (1996) 13748.
[10] S. Kera, H. Setoyama, M. Onoue, K. Okudaira, Y. Harada, N. Ueno, Phys. Rev. B 63 (2001) 115204.
[11] S. Park, Ph.D. Thesis Chemnitz, 2002. Available from: <http://archiv.tu-chemnitz.de/pub/2002/0004/index.html>.
[12] D.R.T. Zahn, G. Salvan, G. Gavrila, B.A. Paez, Adv. Solid State Phys. 45 (2005) 313.
[13] A. Rajagopal, C.I. Wu, A. Kahn, J. Appl. Phys. 83 (1998) 2649.
[14] I.G. Hill, A. Kahn, J. Appl. Phys. 86 (1999) 2116.
[15] R. Schlaf, B.A. Parkinson, P.A. Lee, K.W. Nebesny, N.R. Armstrong, J. Phys. Chem. B 103 (1999) 2984.
[16] A. Nollau, M. Pfeiffer, T. Fritz, K. Leo, J. Appl. Phys. 87 (2000) 4340.
[17] H. Vázquez, W. Gao, F. Flores, A. Kahn, Phys. Rev. B 71 (2005) 041306.
[18] D.R.T. Zahn, T.U. Kampen, H. Méndez, Appl. Surf. Sci. 112–113 (2003) 423.
[19] S. Park, T.U. Kampen, D.R.T. Zahn, W. Braun, Appl. Phys. Lett. 79 (2001) 4124.
[20] T. Chasse, C.-I. Wu, I.G. Hill, A. Kahn, J. Appl. Phys. 85 (1999) 6589.
[21] D.A. Evans, H.J. Steiner, R. Middleton, T.S. Jones, H. Chen, K. Horn, S. Park, T. Kampen, D. Tenne, D.R.T. Zahn, A. Patchett, I.T. McGovern, Appl. Surf. Sci. 175–176 (2001) 374.
[22] M. Knupfer, H. Peisert, Phys. Stat. Sol. (a) 201 (2004) 1055.
[23] T. Schwieger, H. Peisert, M. Knupfer, Chem. Phys. Lett. 384 (2004) 197.
[24] M.L.M. Rocco, K.-H. Frank, P. Yannoulis, E.-E. Koch, J. Chem. Phys. 93 (1990) 6859.
[25] H. Yoshida, K. Tsutsumi, N. Sato, J. Electron Spectrosc. Relat. Phenom. 121 (2001) 83.
[26] I.G. Hill, A. Kahn, Z.G. Soos, R.A. Pascal Jr., Chem. Phys. Lett. 327 (2000) 181.
[27] W. Gao, A. Kahn, Organic Electronics 3 (2002) 53.
[28] M. Knupfer, J. Fink, E. Zojer, G. Leising, D. Fichou, Chem. Phys. Lett. 318 (2000) 585.
[29] E.V. Tsiper, Z.G. Soos, Phys. Rev. B 64 (2000) 195124.
[30] E.V. Tsiper, Z.G. Soos, W. Gao, A. Kahn, Chem. Phys. Lett. 360 (2002) 47.
[31] M. Pope, C.E. Swenberg, Electronic Processes in Organic Crystals, Oxford University Pres, New York, 1982.
[32] W.R. Salaneck, Phys. Rev. Lett. 40 (1978) 60.
[33] Z.G. Soos, E.V. Tsiper, R.A. Pascal Jr., Chem. Phys. Lett. 342 (2001) 652.
[34] T.U. Kampen, G. Gavrila, H. Méndez, D.R.T. Zahn, A. Veary-Roberts, A. Evans, J. Wells, I. McGovern, W. Braun, J. Phys.: Condens. Mat. 15 (2003) S2679.
[35] L.E. Lyons, J. Chem. Soc. (1957) 5001.
[36] D.W. Clack, N.S. Hush, I.S. Woolsey, Inorg. Chim. Acta 19 (1976) 129.
[37] D.R.T. Zahn, T.U. Kampen, S. Hohenecker, W. Braun, Vacuum 57 (2000) 139.
[38] K.C. Prince, Rev. Sci. Instrum. 59 (1988) 741.
[39] P.W. Erdman, E.C. Zipf, Rev. Sci. Instrum. 53 (1982) 225.
[40] J.C. Fuggle, J.E. Inglesfield, Topics in Applied Physics: Unoccupied Electronic States, vol. 69, Editors, Springer-Verlag, Berlin, Heidelberg, 1992.

[41] Th. Gleim, C. Heske, E. Umbach, C. Schumacher, S. Gundel, W. Faschinger, A. Fleszar, Ch. Ammon, M. Probst, H.-P. Steinrück, Surf. Sci. 531 (2003) 77.
[42] Th. Gleim, C. Heske, E. Umbach, C. Schumacher, W. Faschinger, Ch. Ammon, M. Probst, H.-P. Steinrück, Appl. Phys. Lett. 78 (2001) 1867.
[43] A. Curioni, M. Boero, W. Andreoni, Chem. Phys. Lett. 294 (1998) 263.
[44] M.J. Frisch, G.W. Trucks, H.B. Schlegel, G.E. Scuseria, M.A. Robb, J.R. Cheeseman, V.G. Zakrzewski, J.A. Montgomery, R.E. Stratmann, J.C. Burant, S. Dapprich, J.M. Millam, A.D. Daniels, K.N. Kudin, M.C. Strain, O. Farkas, J. Tomasi, V. Barone, M. Cossi, R. Cammi, B. Mennucci, C. Pomelli, C. Adamo, S. Clifford, J. Ochterski, G.A. Petersson, P.Y. Ayala, Q. Cui, K. Morokuma, D.K. Malick, A.D. Rabuck, K. Raghavachari, J.B. Foresman, J. Cioslowski, J.V. Ortiz, B.B. Stefanov, G. Liu, A. Liashenko, P. Piskorz, I. Komaromi, R. Gomperts, R.L. Martin, D.J. Fox, T. Keith, M.A. Al-Laham, C.Y. Peng, A. Nanayakkara, C. Gonzalez, M. Challacombe, P.M.W. Gill, B.G. Johnson, W. Chen, M.W. Wong, J.L. Andres, M. Head-Gordon, E.S. Replogle, J.A. Pople, Gaussian'98 (Revision A.1), Gaussian Inc., Pittsburgh, PA, 1998.
[45] J. Cornil, S. Vanderdonckt, R. Lazzaroni, D.A. Dos Santos, G. Thys, H.J. Geise, L.M. Yu, D.L. Szablewski, D. Bloor, M. Lögdlund, W.R. Salaneck, N.E. Gruhn, D.L. Lichtenberger, P.A. Lee, N.R. Armstrong, J.L. Brédas, Chem. Mater. 11 (1999) 2436.
[46] G. Klebe, F. Graser, E. Hädicke, J. Berndt, Acta Crytallogr. Sect. B: Struct. Sci. B 45 (1989) 69.
[47] H. Hotop, W.C. Lineberger, J. Phys. Chem. Ref. Data 14 (1975) 731.
[48] R.C. Bilodeau, J. Phys. B 31 (1998) 3885.
[49] H. Peisert, M. Knupfer, J. Fink, Appl. Phys. Lett. 81 (2002) 2400.
[50] O.D. Gordan, M. Friedrich, D.R.T. Zahn, Organic Electronics 5 (2004) 291.
[51] O.D. Gordan, M. Friedrich, W. Michaelis, R. Kröger, T.U. Kampen, D. Schlettwein, D.R.T. Zahn, J. Mater. Res. 19 (2004) 2008.
[52] O.D. Gordan, M. Friedrich, D.R.T. Zahn, Thin Solid Films 455–456 (2004) 551.